Geosciences Journal
Vol. 14, No. 4, p. 329 − 333, December 2010
DOI 10.1007/s12303-010-0038-9

Regional moment tensor determination in the southern Korean Peninsula

Junkee Rhie
Seongryong Kim*
School of Earth and Environmental Sciences, Seoul National University, Seoul 151-747, Republic of Korea

ABSTRACT: The Korean Peninsula is a quiet region in terms of seismic activity. Although there are historical records of many large earthquakes that caused severe damage, such major events have not been frequent in recent times, with just a few small- and moderate-sized earthquakes (M ≥ 3) occurring each year. Therefore, the precise analysis of small- to moderate-sized earthquakes is important to understand the characteristics of earthquakes in this region. Broadband seismometers have been deployed in South Korea since 1998 in continually increasing numbers. The current broadband seismic network in Korea is quite dense, and its spatial distribution is nearly homogeneous. This network provides high-quality waveform data and makes moment tensor determination of moderate-sized earthquakes possible. We have inverted regional three-component broadband seismic data for the source parameters of 26 earthquakes ranging in size from Mw 3.2 to 5.0. The moment tensor solutions obtained from time domain waveform inversion show that most of these events have strike-slip faulting mechanisms and that their pseudo P-axis directions are predominantly ENE-WSW, with an average azimuth of 72.77°. The source parameters and maximum horizontal shear stress directions obtained in this study can provide basic information that can act as a foundation for detailed seismotectonic studies and seismic hazard analyses.

Key words: moment tensor, Korean Peninsula

1. INTRODUCTION

In case of large earthquakes, the seismic waveforms are sufficiently strong to be analyzed at teleseismic distances. The Global Centroid Moment Tensor (CMT) project (Dziewonski et al., 1981; Dziewonski and Woodhouse, 1983) and the United States Geological Survey (USGS) (Sipkin, 1982, 1986; Sipkin and Needham, 1993) routinely provide the source parameters of large earthquakes, which are obtained using teleseismic waveforms. However, for small- to moderate-sized earthquakes, regional data are required in order to determine the source parameters. Routine source parameter analysis using regional waveforms is widely carried out in the Western United States (Romanowicz et al., 1993), Japan (Kubo et al., 2002), and Europe (Braunmiller et al., 2002), where dense seismic networks are in operation. Most earthquakes that occur in and around the Korean Peninsula are too small for teleseimic analysis. However, it can be possible to determine the source parameters of small- to moderate-sized earthquakes due to the high-quality regional broadband seismic network which has been deployed since 1998. There have been several previous studies on the source parameters of Korean earthquakes, the first of which was conducted by Jun (1991). Because of the lack of regional waveform data, he used teleseismic body waves to estimate the size, focal mechanism, hypocentral depth, and source duration of 4 relatively large earthquakes (Mw = 5.0–6.0) that occurred in the region. Since then, the source parameters of several local earthquakes have been determined using traditional P-wave first-motion approaches (Baag et al., 1998; Chung and Kim, 2000; Kang and Baag, 2004; Jo and Baag, 2007) and waveform inversion techniques (Kim and Kraeva, 1999; Kim et al., 2000; Park and Mori, 2005) using local seismic data. Recently, Park et al. (2007) determined the focal mechanisms of 71 earthquakes (M_L = 1.9–5.2) in the southern Korean Peninsula using P-wave first motions and SH/P amplitude ratios. Their work was the first effort that systematically estimated the fault plane solutions of small- to moderate-sized earthquakes in Korea. However, traditional first-motion solutions are strongly dependent on the azimuthal station coverage. In case of offshore earthquakes, the solutions can be unstable because of the poor azimuthal coverage of the stations. Moreover, first-motion solutions can only resolve the faulting type of the initial fault break, which is not necessarily consistent with the major faulting. Therefore, the first-motion fault plane solutions can sometimes differ from the moment tensor solutions (Scott and Kanamori, 1985; Anderson, 1988). Compared to traditional first-motion solutions, moment tensor inversion that uses the complete information contained in the seismograms can reflect the major faulting type, an approach that is less dependent on the station coverage. In this paper, we determined the deviatoric moment tensor solutions and centroid depths of 26 earthquakes using a time domain waveform inversion technique (Dreger and Helmberger, 1993; Pasyanos et al., 1996).

2. DATA AND METHODS

Most of the broadband seismic stations in South Korea are operated by either the Korea Meteorological Administration (KMA) or Korea Institute of Geosciences and Mineral Resources (KIGAM). All the KMA stations are equipped

*Corresponding author: srk@snu.ac.kr

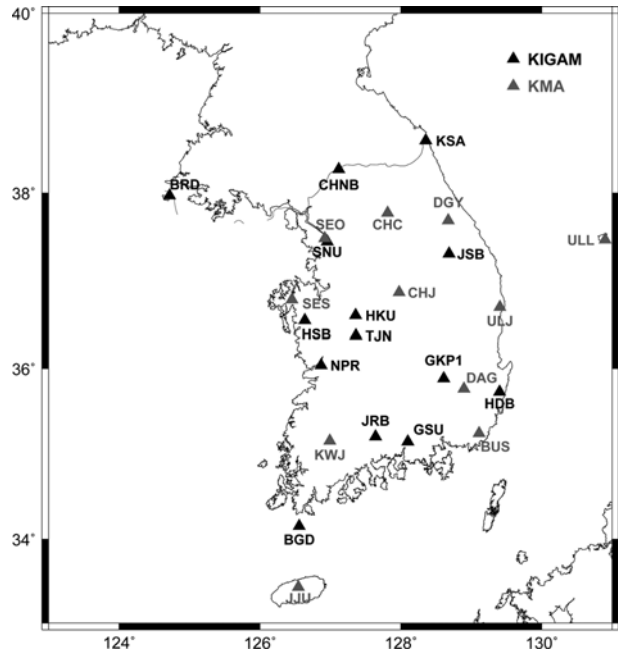

Fig. 1. Location map of broadband seismic stations in South Korea. Black and gray triangles indicate KIGAM and KMA stations, respectively.

with STS-2 broadband sensors, and all the KIGAM stations are equipped with STS-2 or CMG-3TB sensors. Broadband waveform data for local events are available within a few hours after their occurrence. Figure 1 shows the distribution of broadband stations in South Korea. We collected all the available waveform data for local earthquakes ranging in size from M_L 3.5 to 5.1 based on the KIGAM catalog during the time period from 2001 to 2008. Because the distribution of broadband stations before 2001 was too sparse to provide good azimuthal coverage, we considered only earthquakes that took place after 2001. The source parameters for the 26 events are listed in Table 1.

We deconvolved the response of an instrument to displacement. The displacement waveforms were filtered and resampled at intervals of 1 s. The signal-to-noise ratios for small earthquakes are very poor for long periods because they tend not to radiate long-period seismic energy. After testing various pass bands, we selected an optimal pass band (10 s < T < 20 s) for most of the events. However, we used a relatively longer-period band (20 s < T < 50 s) for the largest event (20040526) because it radiates strong long-period energy and the signal-to-noise ratio at a given

Table 1. List of source parameters for 26 events

Event ID (yymmdd)	Origin Time (UTC)	Lat. (°N)	Lon. (°E)	Depth (km)	M_w	Strike	Dip	Rake	VR (%)	Stations
20011121	01:49:11.60	36.70	128.34	13	3.5	15; 118	66; 64	64; 151	85.8	ULJ, SEO
20011124	07:10:32.00	36.73	129.85	11	3.9	308; 215	77; 76	15; 166	92.6	GKP1, KWJ, SNU
20020317	00:25:57.10	38.10	124.56	7	3.7	54; 234	55; 35	–90; –90	84.5	CHNB, SNU, TJN
20020708	19:01:49.90	35.86	129.79	15	3.7	125; 31	78; 74	16; 168	78.7	BUS, DAG, CHJ, CHC
20020917	09:08:11.80	36.47	124.02	5	3.4	223; 129	79; 67	–157; –12	73.3	BRD, HKU, BGD
20021209	22:42:49.80	38.86	127.26	9	3.7	297; 28	84; 81	–9; –174	84.0	DGY, CHC, SEO
20030109	08:33:21.20	37.53	124.57	7	3.8	180; 270	84; 84	174; 6	88.8	BRD, SNU, SES
20030322	20:38:39.70	34.86	124.35	17	4.8	204; 294	87; 85	175; 3	84.8	BRD, SES, KWJ
20030330[a]	11:10:55.98	37.57	123.82	5	4.7	278; 52	56; 44	–60; –127	80.4	SNU, SES, NPR, KWJ
20030415	17:55:23.90	36.44	126.17	3	3.4	178; 297	81; 81	105; 30	77.6	CHC, HKU, KWJ
20030609	01:14:00.00	35.92	123.63	11	3.9	207; 299	85; 72	162; 5	75.2	BRD, SNU, BGD
20031013	09:12:04.90	36.99	126.48	13	3.8	296; 26	90; 84	–6; –180	94.5	CHC, CHJ, HKU, KWJ
20040426	04:29:25.40	35.82	128.24	9	3.6	140; 31	73; 45	48; 155	93.4	ULJ, BUS, KWJ, TJN, CHJ
20040529	10:14:24.70	36.66	130.10	9	5.0	356; 175	46; 44	91; 89	96.9	BUS, GKP1, CHJ, DGY
20040601	11:22:17.30	37.08	130.23	21	3.7	44; 306	74; 64	–153; –18	83.0	DAG, ULJ, DGY
20040805	20:32:53.29	35.86	127.33	9	3.2	122; 32	86; 81	9; 176	79.8	DAG, BUS, KWJ, SES
20050614	22:07:04.16	33.31	125.96	11	3.8	5; 274	85; 82	–172; –5	90.5	KWJ, BUS
20050629	14:18:03.80	34.40	129.18	7	4.1	19; 133	70; 42	128; 31	90.5	JJU, BGD, KWJ, BUS
20051009	23:51:08.30	37.78	124.95	9	3.6	23; 256	59; 45	–125; –46	88.5	CHC, SNU, SES
20060119	03:35:35.49	37.20	128.78	7	3.5	123; 202	86; 76	–14; –178	87.4	ULJ, DAG, TJN, CHC
20060403	09:14:03.46	38.85	126.01	11	3.3	136; 227	88; 71	–19; –178	73.9	CHC, BRD
20060513	10:14:32.69	34.14	129.04	3	3.7	310; 86	51; 48	–59; –122	79.2	NPR, TJN, HKU
20070120	11:56:53.60	37.69	128.58	11	4.6	204; 294	88; 88	178; 2	96.0	ULJ, DAG, TJN, SEO
20080116	10:58:01.63	35.58	125.32	7	3.9	298; 29	87; 86	–4; –177	90.1	SES, TJN, KWJ, BGD
20080229	06:53:00.95	38.83	126.21	7	3.4	17; 282	81; 63	–153; –10	74.3	KSA, CHC
20080531	12:59:32.56	33.54	125.72	21	4.0	201; 110	86; 79	–169; –4	92.3	BGD, JJU

[a]USGS PDE

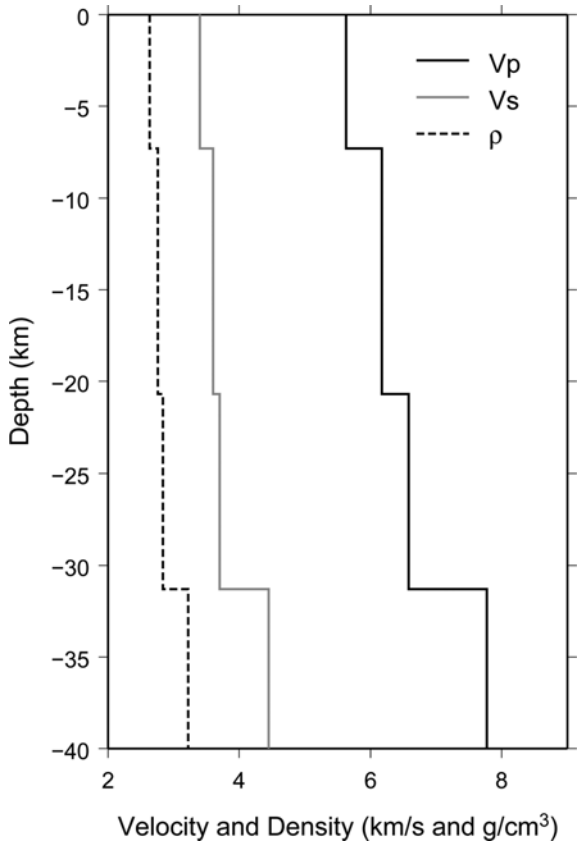

Fig. 2. One-dimensional velocity and density models used for Green's function computations.

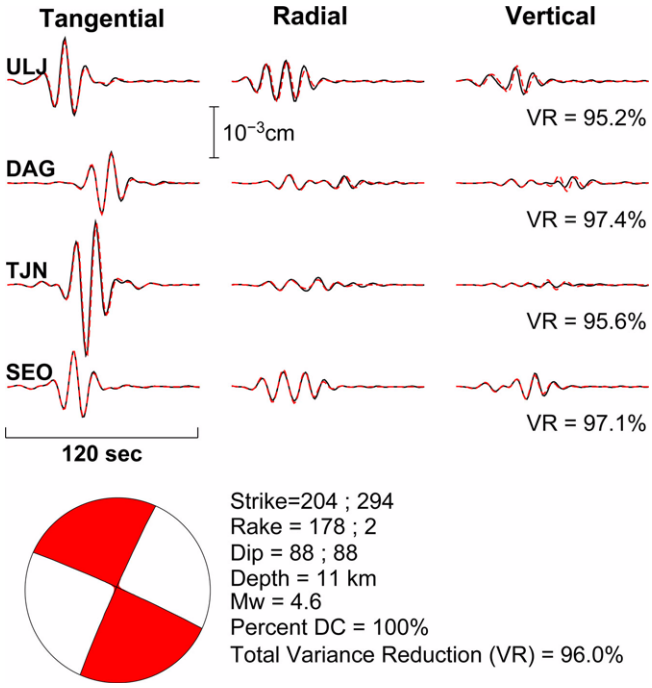

Fig. 3. Example of moment tensor inversion of event 20070120. The black and red traces indicate the observed and synthetic waveforms calculated for a given moment tensor solution and the 1D velocity model, respectively.

period band is high.

Green's functions were computed using a frequency-wave number integration method developed by Saikia (1994). The 1D seismic velocity model for the Green's function computation was obtained from a previous study based on waveform modeling (Kim et al., unpublished). Figure 2 shows the 1D velocity model used for the Green's function computations. For a given velocity model, a catalog of Green's functions was constructed for a distance range between 5 and 500 km in increments of 5 km and for a source depth between 1 and 25 km in increments of 2 km. Because we computed Green's functions for discrete epicentral distances, it is highly probable that the actual epicentral distances are slightly different from those for Green's functions. To compensate for any errors caused by this possible discrepancy in epicentral distances, unmodeled propagation effects, and event mislocations, Green's functions and observed waveforms were aligned using cross-correlation before the inversion. The observed waveform data were selected by considering the azimuthal coverage and quality of the data, and we then inverted the complete three-component waveform data for the deviatoric moment tensor solution by minimizing the least square misfit between the synthetic and observed waveforms (Fig. 3). In addition, the centroid depth was determined by a grid search over the prescribed trial depths. The event locations listed in the KIGAM catalog were used for the waveform inversion (Table 1). However, we found that the moment tensor solution was not well determined for one event (20030330) with a relatively large magnitude (M_L = 4.8). For this event, we tested alternative epicenters taken from the KMA and USGS PDE (Preliminary Determination of Epicenters) catalogs. In the end, we used the USGS PDE for this event because the USGS source information provided the best result compared to the others.

3. RESULTS AND DISCUSSION

The moment tensor solutions for all events were well determined, and their moment magnitudes, best double couple solutions, and centroid depths are listed in Table 1. Our moment tensor solutions show that most of the events involve strike-slip mechanisms, except for several events that occurred in the Yellow Sea and East Sea (Fig. 4). The faulting types of the events were determined based on the plunges of the principal stresses (Table 3 in Zoback, 1992). Although one event (20030415) was assigned to an unknown stress regime, we inspected its plunge angles and determined that the most appropriate category is thrust faulting. Thus, all events were assigned to four stress regimes: normal faulting (NF), strike-slip faulting (including a minor normal or thrust component) (SS), thrust faulting (TF), and a predominant thrust with a strike-slip component (TS). The

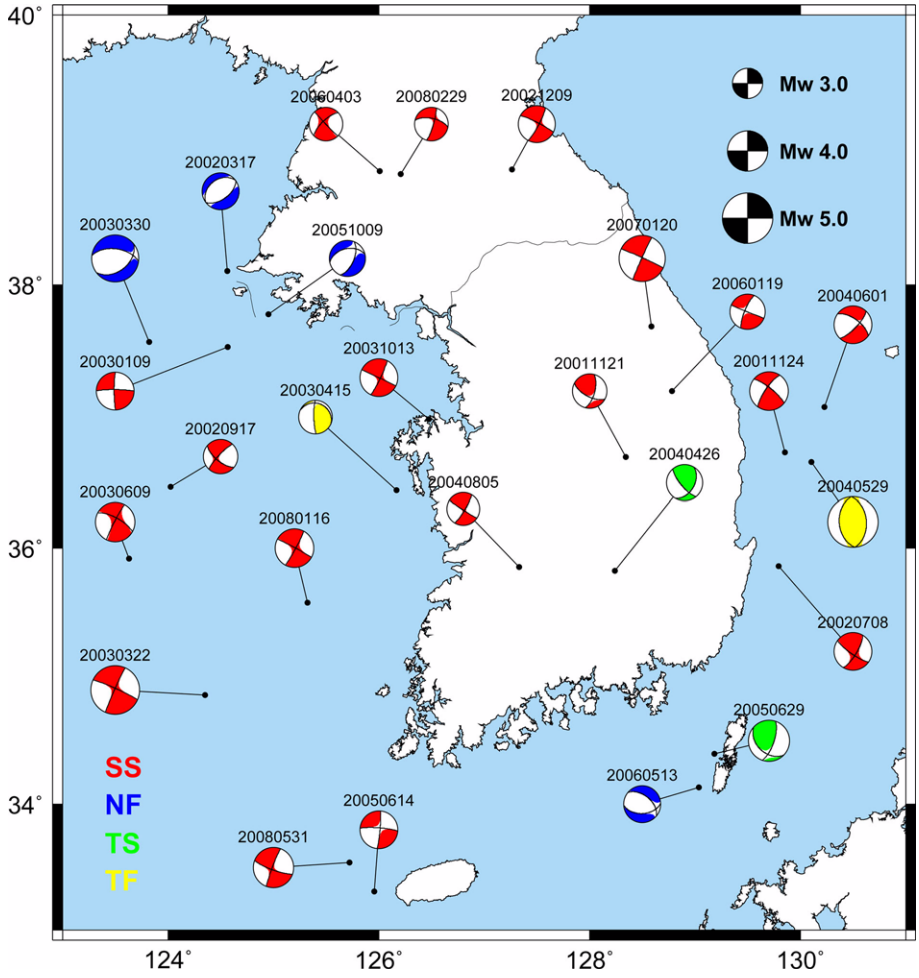

Fig. 4. Map of moment tensor solutions. NF (blue): normal faulting, SS (red): strike-slip faulting (including a minor normal or thrust component), TF (yellow): thrust faulting, and TS (green): a predominant thrust with a strike-slip component.

stress regimes of the events are indicated by different colors in Figure 3. Most of the earthquakes (18 out of 26) belong to the SS stress regime, and the other earthquakes with different stress regimes were scattered throughout our study area, except for three NF events clustered around the BRD station (Fig. 4). We also found that there was another SS event (20030109) near the clustered NF events. This may indicate that the magnitudes of the vertical (S_v) and maximum horizontal stress (S_{Hmax}) are similar in this small region (Zoback, 1992). To investigate the regional stress fields in our study area, we calculated the pseudo P-axes (horizontally projected P-axes) of the events (Fig. 5) based on the stress regimes (Zoback, 1992). The pseudo P-axis directions represent the directions of the horizontal maximum strain and also correspond to the directions of S_{Hmax}. It should be noted here that the normal and reverse-type events agree with the S_{Hmax} direction, which can be slightly different for strike-slip events. The average azimuth of all the pseudo P-axes is 72.77° (or 252.77°), and the standard deviation is only 14.46°. Such a small standard deviation implies that the S_{Hmax} directions are more or less uniform throughout the entire area. Although several S_{Hmax} directions, particularly for the earthquakes in the northwestern

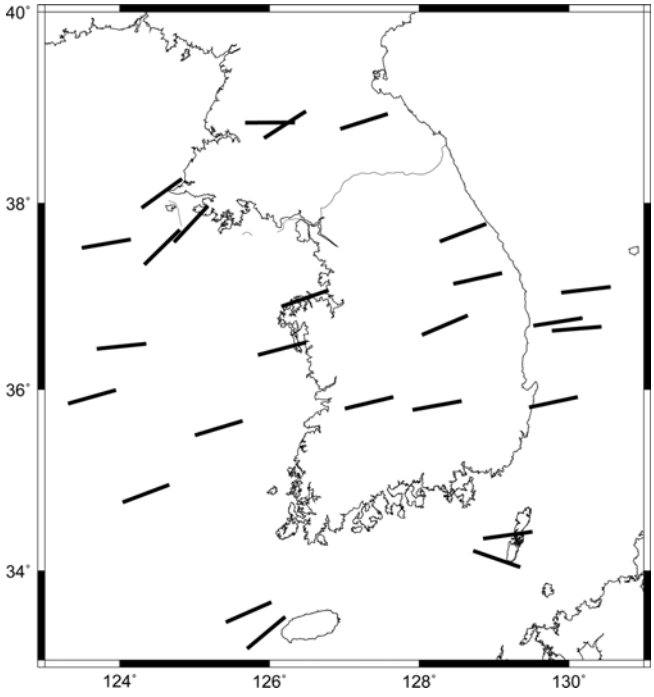

Fig. 5. Distribution of azimuth directions of horizontally projected P-axis (pseudo P-axis).

part of the study region, may have azimuth values considerably different from the average value, it is difficult to verify whether these differences reflect significant changes in the regional stress fields. More reliable regional stress tensors can be determined from the stress tensor inversion (e.g., Angelier, 1979; Gephart and Forsyth, 1984) when many P- and T-axis direction data are available for a small area. Unfortunately, the spatial distribution of the events used in this study is not sufficiently dense to perform stress inversion calculations. However, an estimated average azimuth of S_{Hmax} is consistent with the orientation of the principal horizontal axis of the strain rate tensors obtained from GPS measurements in the same area (Jin et al., 2006). These consistent observations from different datasets support the high degree of reliability of our estimate, and they may indicate that the feature of the convergence continental margin around the border of Eurasia and Pacific plates. Although more moment tensor solutions would be necessary in order to investigate the regional stress tensors and their spatial variations, our results can be useful for roughly delineating the stress fields and faulting types of earthquakes in and around the Korean Peninsula.

ACKNOWLEDGMENTS: We thank the KMA and KIGAM for providing us with broadband seismic data. This work was funded by the Korea Meteorological Administration and Development Program under Grant CATER 2008-5113.

REFERENCES

Anderson, H., 1988, Comparison of centroid-moment tensor and first motion solutions for western Mediterranean earthquake. Physics of the Earth and Planetary Interiors, 52, 1–7.

Angelier, J., 1979, Determination of the mean principal directions of stresses for a given fault population. Tectonophysics, 56, T17–T26.

Baag, C.-E., Shin, J.S., Chi, H.C., Kang, I.B., and Ryoo, Y., 1998, Fault plane solutions of the December 13, 1996 Yeongweol earthquake. Journal of the Korean Geophysical Society, 1, 23–30 (in Korean with English abstract).

Braunmiller, J., Kradolfer, U., Baer, M., and Giardini, D., 2002, Regional moment tensor determination in the European-Mediterranean area – initial results. Tectonophysics, 356, 5–22.

Chung, T.W. and Kim, W., 2000, Fault plane solutions for the June 26, 1997 Kyong-ju Earthquake. Journal of the Korean Geophysical Society, 3, 245–250 (in Korean with English abstract).

Dreger, D.S. and Helmberger, D.V., 1993, Determination of source parameters at regional distances with single station or sparse network data. Journal of Geophysical Research, 98, 8107–8125.

Dziewonski, A.M. and Woodhouse, J.H., 1983, An experiment in the systematic study of global seismicity: centroid moment-tensor solutions for 201 moderate and large earthquakes of 1981. Journal of Geophysical Research, 88, 3247–3271.

Dziewonski, A.M., Chou, T.-A., and Woodhouse, J.H., 1981, Determination of earthquake source parameters from waveform data for studies of global and regional seismicity. Journal of Geophysical Research, 86, 2825–2852.

Gephart, J.W. and Forsyth, D.W., 1984, An improved method for determining the regional stress tensor using earthquake focal mechanism data: application to the San Fernando earthquake sequence. Journal of Geophysical Research, 89, 9305–9320.

Jin, S., Li, Z.C., and Park, P.-H., 2006, Seismicity and GPS constraints on crustal deformation in the southern part of the Korean Peninsula. Geosciences Journal, 10, 491–497.

Jo, N. and Baag, C.-E., 2007, The 20 January 2007, Mw 4.5 Odaesan, Korea, earthquake. Geosciences Journal, 11, 51–58.

Jun, M.-S., 1991, Body-wave analysis for shallow intraplate earthquakes in the Korean Peninsula and Yellow Sea. Tectonophysics, 192, 345–357.

Kang, T.-S. and Baag, C.-E., 2004, The 29 May 2004, Mw=5.1, offshore Uljin earthquake, Korea. Geosciences Journal, 8, 114–123.

Kim, S.G. and Kraeva, N., 1999, Source parameter determination of local earthquakes in Korea using moment tensor inversion of single station data. Bulletin of the Seismological Society of America, 89, 1077–1082.

Kim, S.G., Kraeva, N., and Chen, Y.-T., 2000, Source parameter determination of regional earthquakes in the Far East using moment tensor inversion of single-station data. Tectonophysics, 317, 125–136.

Kubo, A., Fukuyama, E., Kawai, H., and Nonomura, K., 2002, NIED seismic moment tensor catalogue for regional earthquakes around Japan: quality test and application. Tectonophysics, 356, 23–48.

Park, J.-C., Kim, W., Chung, T. W., Baag, C.-E., and Ree, J.-H., 2007, Focal mechanisms of recent earthquakes in the Southern Korean Peninsula. Geophysical Journal International, 169, 1103–1114.

Park, S.-C. and Mori, J., 2005, Source parameter of the May 29, 2004 South Korea earthquake (M_L 5.2). Earth Planets Space, 57, 471–475.

Pasyanos, M.E., Dreger, D.S., and Romanowicz, B., 1996, Toward real time estimation of regional moment tensors. Bulletin of the Seismological Society of America, 86, 1255–1269.

Romanowicz, B., Dreger, D., Pasyanos, M., and Uhrhammer, R., 1993, Monitoring strain release in central and northern California using broadband data. Geophysical Research Letters, 22, 1643–1646.

Saikia, C.K., 1994, Modified frequency-wavenumber algorithm for regional seismograms using Filon's quadrature: modeling of Lg waves in eastern North America. Geophysical Journal International, 118, 142–158.

Scott, D.R. and Kanamori, H., 1985, On the consistency of moment tensor source mechanisms with first-motion data. Physics of the Earth and Planetary Interiors, 37, 97–107.

Sipkin, S.A., 1982, Estimation of earthquake source parameters by the inversion of wave-form data: synthetic waveforms. Physics of the Earth and Planetary Interiors, 30, 242–259.

Sipkin S.A., 1986, Estimation of earthquake source parameters by the inversion of waveform data: global seismicity, 1981–1983. Bulletin of the Seismological Society of America, 76, 1515–1541.

Sipkin, S.A. and Needham, R.E. 1993, Moment-tensor solutions estimated using optimal filter theory: global seismicity. Physics of the Earth and Planetary Interiors, 75, 199–204.

Zoback, M.L., 1992, First- and second-order patterns of stress in the lithosphere: The World Stress Map Project. Journal of Geophysical Research, 97, 11703–11728.

Manuscript received September 17, 2010
Manuscript accepted December 7, 2010